Drug Delivery

DOI: 10.1002/ange.201311133

An Activatable Theranostic for Targeted Cancer Therapy and Imaging**

Sankarprasad Bhuniya, Sukhendu Maiti, Eun-Joong Kim, Hyunseung Lee, Jonathan L. Sessler, Kwan Soo Hong,* and Jong Seung Kim**

Abstract: *A new theranostic strategy is described. It is based on the use of an "all in one" prodrug, namely the biotinylated piperazine-rhodol conjugate* ***4a****. This conjugate, which incorporates the anticancer drug SN-38, undergoes self-immolative cleavage when exposed to biological thiols. This leads to the tumor-targeted release of the active SN-38 payload along with fluorophore* ***1a****. This release is made selective as the result of the biotin functionality. Fluorophore* ***1a*** *is 32-fold more fluorescent than prodrug* ***4a****. It permits the delivery and release of the SN-38 payload to be monitored easily in vitro and in vivo, as inferred from cell studies and ex vivo analyses of mice xenografts derived from HeLa cells, respectively. Prodrug* ***4a*** *also displays anticancer activity in the HeLa cell murine xenograft tumor model. On the basis of these findings we suggest that the present strategy, which combines within a single agent the key functions of targeting, release, imaging, and treatment, may have a role to play in cancer diagnosis and therapy.*

Theranostics refers to an appealing new approach to drug development wherein therapeutic modalities are combined with those associated with diagnostic imaging. If successfully implemented, theranostic strategies could permit the concurrent monitoring and treatment of a particular disease, while permitting increased insights into drug delivery kinetics, local response, and overall efficacy. Ultimately, theranostics could allow treatment protocols to be adjusted to the needs of individual patients in a way that thus far has not been generally possible. By going beyond the current "one size fits all" concept associated with most current drug development efforts, theranostic approaches could help move the field of medicine toward an era of more effective and personalized treatment.[1] For this promise to be realized, advances in imaging, targeting, and therapy must be made and effective targeting and release strategies must be developed. Herein, we report an activatable prodrug strategy wherein a biotinylated piperazine-rhodol is combined with the topoisomerase I inhibitor, SN-38. This combination permits targeted imaging and cytotoxicity in cellular cancer models. It also allows for tumor-selective localization and antitumor activity in mouse xenografts.

As we conceive it, a number of elements need to be optimized to create a functioning theranostic that would be attractive for use in cancer treatment protocols. These include the imaging modality, the choice of active therapeutic agent, and tumor targeting. A scission strategy that permits the concurrent release of the signaling and therapeutic agent would also be beneficial from an operational perspective. Such an approach is especially attractive for cancer treatment, as a number of enzymes overexpressed in malignant cells[2] have a cleavage activity that could be conveniently used to activate a prodrug via bond scission. When complemented by the use of ligands selective for a specific cell type, a combination of targeting and drug release should be possible that is highly effective.[3] If fluorophores[4] are included within the theranostic design, real-time monitoring by fluorescence imaging should be possible. Based on this strategy, we recently developed a theranostic prodrug system based on Gemcitabine where a biotin subunit was incorporated as a potential localizer and coumarin was used as the fluorophore.[5] While this system permitted in vitro imaging, tumor localization was not demonstrated in vivo.

Here, we describe a prodrug (**4a** in Scheme 1) that is based on the topoisomerase I inhibitor, SN-38. This inhibitor is the active ingredient in CPT11 (camptothecin), a therapeutic agent used to treat various carcinomas,[6] and is one of the most efficient drugs in this class.[7] The use of a biotin subunit provides for tumor localization,[8] whereas a piperazine-rhodol permits fluorescent-based monitoring both in vitro and in vivo. A further key design feature of the present theranostic is the use of a labile, self-immolative linker based on disulfide bonds that permits release of both the active SN-38 therapeutic agent and the N-biotinylated piperazine-rhodol fluorophore in the presence of intracellular thiols. To the best of our knowledge, this is the first system where drug targeting, release, and fluorescence-based monitoring have been demonstrated in an animal model.

[*] Dr. S. Bhuniya,[+] Dr. E. J. Kim,[+] H. Lee, Dr. K. S. Hong
Division of MR Research, Korea Basic Science Institute
Cheongwon 363-883 (Korea)
E-mail: kshong@kbsi.re.kr
Dr. S. Maiti,[+] Prof. J. S. Kim
Department of Chemistry, Korea University
Seoul 136-701 (Korea)
E-mail: jongskim@korea.ac.kr
Prof. J. L. Sessler
Department of Chemistry, University of Texas at Austin
Austin, TX 78712-1224 (USA)
E-mail: sessler@cm.utexas.edu

[+] These authors contributed equally to this work.

[**] This work was supported by the Creative Research Initiative program (No. 2009-0081566) of National Research Foundation of Korea, the CAP (PBC066) funded by the Korea Research Council of Fundamental Science and Technology, and by a grant from the Korea Basic Science Institute (D33400).

Supporting information for this article is available on the WWW under http://dx.doi.org/10.1002/anie.201311133.

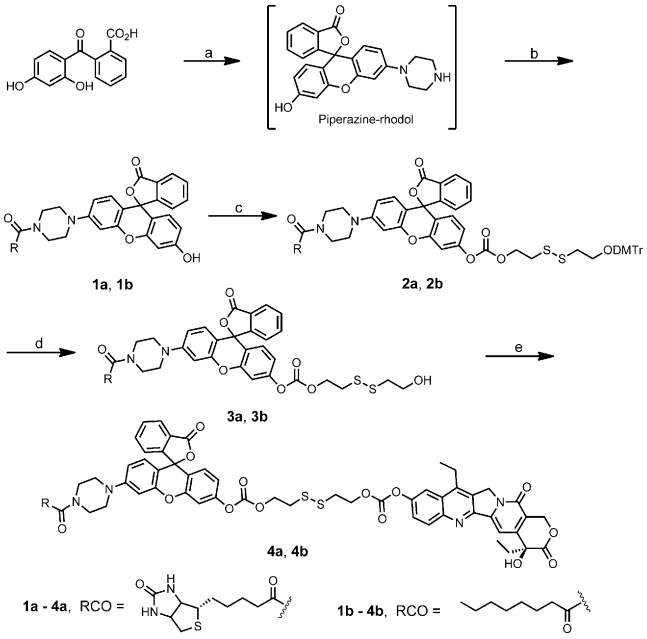

Scheme 1. Synthesis of theranostic prodrugs **4a,b**. Reagent and reaction conditions: a) 1-(3-hydroxyphenyl)-piperazine, TFA, pressure tube, 95 °C, 3 h; b) RCO_2H, EDCI, DMAP, DMF, RT, 12 h; c) mono-*O*-dimethoxytrityl-2-hydroxyethyl disulfide, 4-nitrophenyl chloroformate, DIPEA, DCM, 0 °C–RT, 3 h then **1a,b**, TEA, DMF, RT, 24 h; d) DCM, AcOH, RT, 24 h; e) 4-nitrophenyl chloroformate, DIPEA, DCM, 0 °C–RT, 3 h then SN-38, TEA, DMF, RT, 24 h. TFA = trifluoroacetic acid; EDCI = *N*′-(3-dimethylaminopropyl)-*N*-ethylcarbodiimide; DMAP = 4-dimethylaminopyridine; DIPEA = diisopropylethylamine; DCM = dichloromethane; TEA = triethylamine.

The theranostic prodrug **4a** was synthesized as outlined in Scheme 1. The piperazine-rhodol was prepared as previously described.[9]

The biotin-containing fluorescent precursor **1a** was obtained by reaction of biotin with the crude piperazine-rhodol, followed by amide coupling. Next, mono-*O*-DMTr-2-hydroxyethyl disulfide was reacted with 4-nitrophenyl chloroformate, followed by reaction with **1a**; this gave compound **2a** in moderate yield. Removal of the *O*-DMTr protecting group gave **3a** in 60% yield. Compound **3a** was then reacted with 4-nitrophenyl chloroformate to give a reactive intermediate, which was subsequently reacted with SN-38 to give the prodrug target **4a**. The non-targeted prodrug **4b** was also synthesized as a reference compound so as to judge the cell specificity of **4a**. Detailed synthetic procedures, including spectroscopic data, are provided in the experimental section.

Before proceeding to cell imaging experiments, we explored whether a biologically relevant thiol was able to induce cleavage of the disulfide bond in prodrug **4a**. Towards this end conjugate **4a** was treated with glutathione (GSH) under physiological conditions. The changes in the optical features were then monitored using UV/Vis and fluorescence spectroscopy. As prepared, prodrug **4a** (15.0 μM in PBS (phosphate-buffered saline) containing 25% DMSO (dimethyl sulfoxide)) exhibits a strong absorption peak at $\lambda_{max} = 510$ nm in its absorption spectrum. This peak increases in intensity by ca. 25-fold upon the addition of GSH (5.0 mM). The fluorescence emission signal corresponding to **4a** (5.0 μM in PBS containing 25% DMSO) at $\lambda_{max} = 544$ nm (excitation at $\lambda_{max} = 510$ nm) was also enhanced by ca. 32-fold following exposure to GSH (5.0 mM) as shown in Figure 1b. As expected for a system undergoing S–S bond cleavage and release of an active fluorophore, the emission spectrum of the solution of **4a** + GSH proved identical to that for the reference fluorescent system **1a** recorded at the same

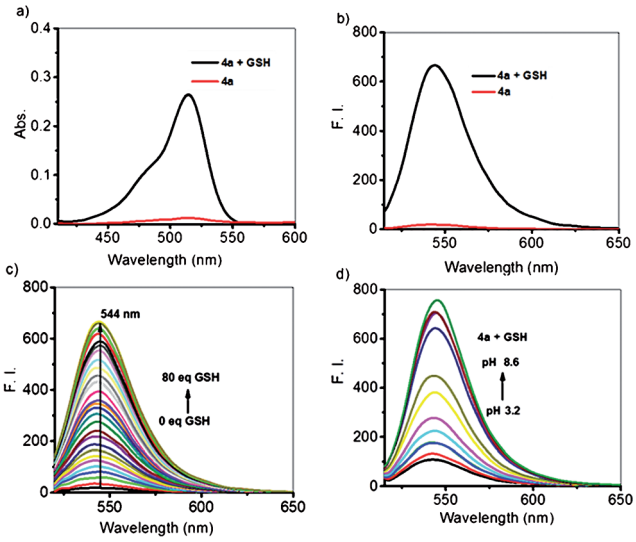

Figure 1. a) Absorption spectra of **4a** (15.0 μM in PBS, 25% DMSO) recorded in the presence and absence of GSH (5.0 mM). b) Fluorescence spectra of **4a** (5.0 μM) recorded in the presence and absence of GSH (5.0 mM). c) Fluorescence changes of **4a** (5.0 μM) after treatment with increasing concentrations of GSH (0–80 equiv). d) Fluorescence spectra of **4a** (5.0 μM) recorded in the presence of GSH (5.0 mM) as a function of pH. Excitation was effected at 510 nm with the excitation and emission slit widths both set at 3 nm.

concentration (Figure S1 in the Supporting Information). We also observed that in the presence of 80 equiv GSH, the fluorescence intensity reached saturation (Figure 1c). These results are fully consistent with the design expectation that the disulfide bond of **4a** is readily cleaved by GSH.

Since GSH and other reduced thiols are present in cancer cells,[10] the bond scission seen under the conditions of the above analyses is expected to translate into an increase in the intracellular concentration of SN-38 while also providing an easy-to-monitor fluorescent marker.

We also analyzed the pH-dependent changes in the intensity of the fluorescence emission ($\lambda_{max} = 544$ nm) of **4a** (5.0 μM) in the absence and presence of 5.0 mM GSH. As shown in Figure 1d and S2, in the absence of GSH, no immediate change in the fluorescence features of **4a** are seen over the pH range of 3.2 to 8.6. In the presence of GSH, however, a significant increase in the fluorescence intensity is seen over a pH range of 5 to 8.6 within minutes of mixing (see below for detailed time-course studies). These observations provide further support for the suggestion that prodrug **4a** contains a cleavable linker.

To assess whether other biologically relevant analytes might interfere with the proposed GSH-induced cleavage process in vitro or in vivo, the interaction of **4a** with various metal ions and thiols, thiol-free amino acids were investigated under the same reaction conditions used to test the effect of GSH (Figure 2a and b).

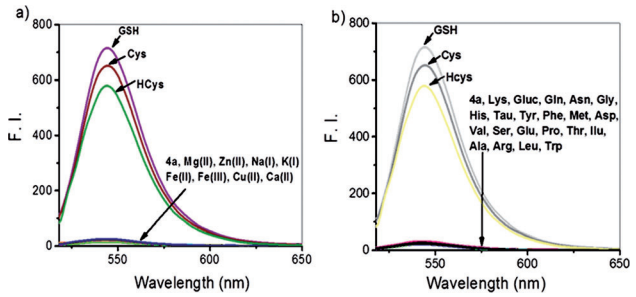

Figure 2. Fluorescence spectra of **4a** (5.0 μM in PBS, 25% DMSO) recorded in the presence and absence of various metal cations (1.0 mM) and GSH, Cys, Hcy (5.0 mM), respectively. Excitation was effected at 510 nm with the excitation and emission slit widths both set at 3 nm.

Addition of cysteine (Cys) or homocysteine (Hcy) to **4a** caused changes in the emission similar to those elicited by GSH. On the other hand, no significant spectroscopic changes were detected upon exposure to thiol-free amino acids or biologically relevant metal cations, including Na^+, K^+, Ca^{2+}, Mg^{2+}, Zn^{2+}, Fe^{2+}, Fe^{3+}, Cu^{2+} respectively. On this basis, we conclude that the disulfide bond in **4a** will undergo specific thiol-mediated cleavage without substantial interference from other chemical entities that would be expected to be prevalent in a biological environment.

The timing of drug release from its prodrug form can have a critical impact on its efficacy.[11] To investigate the time-dependent release of the active drug SN-38 and fluorophore components present in **4a**, the extent of fluorescence signal recovery at $\lambda_{max} = 544$ nm was recorded as a function of time at different GSH concentrations (Figure S3). It was found that the fluorescence intensity reached a maximum and plateaued within 10 min upon exposure to 5 mM GSH. This GSH concentration mimics the average intracellular glutathione level. Thus, this finding leads us to suggest that the active components (fluorophore and drug) will be released shortly after prodrug **4a** enters a cell.

To confirm whether the fluorescence enhancement observed when **4a** is exposed to GSH reflects SN-38 release (as opposed to just the active fluorophore) prodrug **4a** was treated with 5.0 mM GSH at 37 °C for 2 h. An aliquot was then subjected to mass spectrometric (MS) analysis. Molecular mass peaks corresponding to SN-38 (MW = 392.4) and **1a** (MW = 626.3) were observed (Figure S34). This is taken as evidence that the disulfide bond present in **4a** is readily cleaved by GSH and that this cleavage leads to release of free SN-38 along with the fluorescent probe as shown in Scheme 2. Based on the products observed, we suggest this release process involves intramolecular cyclization and concomitant scission of a neighboring carbonate bond.

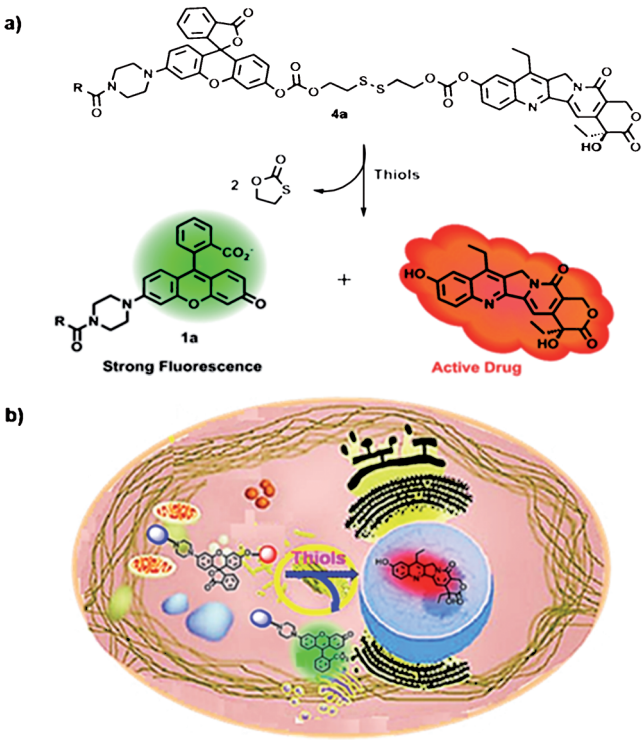

Scheme 2. a) Thiol-induced cleavage of prodrug **4a** and b) schematic representation of its proposed intracellular processing.

To gain insight into whether the cellular uptake of **4a** could be targeted, studies were carried out using biotin receptor-enriched tumor cells. Control studies were conducted using normal NIH3T3 cells that express a low level of the biotin receptor.[12] The precursor **3a** and prodrug **4a** were incubated at various concentrations with HeLa cells over-expressing the biotin receptor[13] for 2 h, and the efficiency of cellular uptake was measured using flow cytometry (Figure 3a).

In the case of both **3a** and **4a** cellular uptake proved concentration-dependent, with plateaus being reached at similar concentration levels for both compounds of 10 μM. Since **4a** contains a potent anti-cancer drug, SN-38, which could induce cytotoxicity and affect the background cellular fluorescence, we used precursor **3a**, rather than **4a**, to follow internalization. As shown in Figure 3b, the biotin receptor-positive HeLa and A549 cancer cell lines exhibited strong fluorescence within 2 h of incubation with **3a** (10 μM). In contrast, a very weak fluorescence signal was observed in the NIH3T3 cells. Such a difference in emission among these cell lines is consistent with the suggestion that the selective uptake of **3a** by HeLa and A549 cells can be attributed to receptor-mediated endocytosis.

Furthermore, as assessed by fluorescence-activated cell sorting (FACS), the uptake of **3a** proved dose-dependent in both the biotin receptor-positive HeLa and receptor-negative NIH3T3 cells, with the uptake in the HeLa cells being routinely more than 3-fold higher than that in the NIH3T3 cells (Figure S4). However, the non-biotinylated precursor **3b** gives rise to random cellular uptake (Figure S5) irrespective

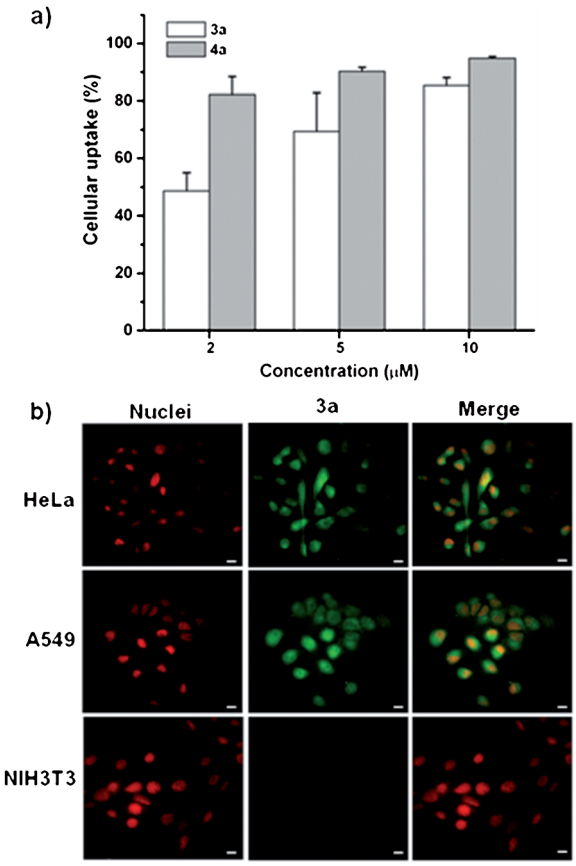

Figure 3. a) Cellular uptake of **3a** and **4a** by HeLa cells as assessed by FACS analysis performed after 2 h incubation. b) Fluorescence images of HeLa, A549, and NIH3T3 cells treated with 10 μM of **3a** in PBS for 2 h. Nuclear counter-staining using DRAQ5 (red). Scale bar, 10 μm. Images were obtained using excitation wavelengths of 510 nm and 630 nm, with the emission being monitored over the 540–600 and 680–750 nm spectral regions for the green and red signals, respectively.

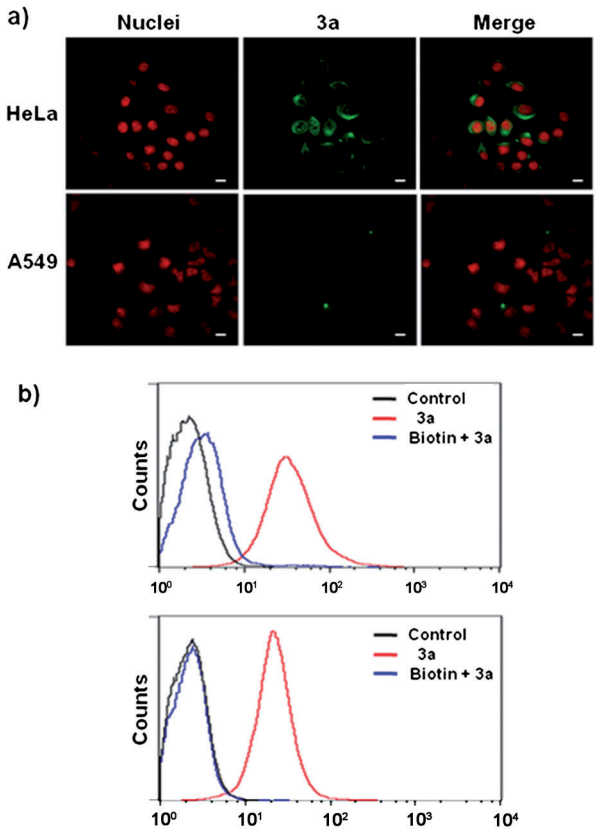

Figure 4. a) Optical images of the biotin receptor-positive HeLa and A549 cells pretreated with biotin (100 μM) for 1 h, followed by incubation with **3a** (10 μM) in PBS for 2 h. b) The reduced cellular uptake efficiency was further demonstrated by FACS analysis. Nuclear counter-staining using DRAQ5 (red). Scale bar: 10 μm. Images were obtained using excitation wavelengths of 510 nm and 630 nm, with the emission being monitored over the 540–600 and 680–750 nm spectral regions for the green and red signals, respectively.

of the cell line chosen for study. This observation leads us to conclude that biotin functionality present in **3a** plays an important role in terms of mediating the cellular uptake of **3a** (or **4a**) depending on the level of overexpressed biotin receptors present in the cancer cells. It is envisioned that **4a** may be a possible tool for the targeted delivery of chemotherapeutic and diagnostic imaging agents to tumor sites.

To provide further confirmation for the proposed endocytosis-mediated uptake mechanism, the biotin receptor-positive HeLa and A549 cells were pre-treated with an excess of biotin prior to incubating with **3a** for 2 h. This treatment was expected to block the receptors and prevent or reduce competitive binding by **3a**. The results of the fluorescence imaging analyses revealed that, in accord with expectations, the number of fluorescent cells was significantly reduced (Figure 4a). Further, the overall fluorescence intensity was significantly decreased (Figure 4b) in the HeLa and A549 cells pretreated with biotin. These findings are thus fully consistent with the suggestion that cellular uptake of precursor **3a** in receptor-positive cells occurs by receptor-mediated endocytosis.[14]

As a test of whether thiol-induced disulfide bond cleavage and the concurrent increase in fluorescence is mediated by thiols within cells, the fluorescence behavior of precursor **3a** was analyzed in HeLa and A549 cells pretreated with *N*-ethylmaleimide (NEM). NEM reacts with thiols and was expected to reduce the effective concentration of GSH (and other free thiols), thus inhibiting the critical S–S scission process.[15] In fact, the intracellular fluorescence ascribed to **3a** was substantially reduced in the presence of 50 μM NEM (Figure S6). On this basis, we conclude that the fluorescence enhancement seen for **3a** in vitro is triggered, at least for the most part, by reaction with intracellular thiols (Scheme 2). It is inferred that the same mode of action holds for **4a**, although because of concerns involving cytotoxicity and artifacts (see above) this was not tested directly.

To determine whether the enhancement in long-wavelength fluorescence intensity observed for prodrug **4a** under conditions of bond scission (cf. Figure 1) can be correlated with intracellular release of SN-38, an effort was made to detect SN-38 directly.[16] Towards this end, lysates of HeLa cells were treated with **4a** (10 μM) and subjected to fluorometric analysis with monitoring effected at 370 nm. This

wavelength corresponds to the UV absorption maximum of SN-38 (Figure S7). In fact, the intensity of the 370 nm and 548 nm emission signals (the latter ascribable to **1a**) were both seen to increase under conditions where S–S bond scission occurs. As a result, we conclude that intracellular release of SN-38 from prodrug **4a** could be monitored by following the increase in the intensity of the easier-to-visualize 548 nm fluorescence emission.

The anti-cancer efficacy of prodrug **4a** and **4b** were evaluated in three cell lines characterized by different expression levels of the biotin receptor.

This was done using standard cell viability protocols. Briefly, cells were treated separately with **4a** and **4b**, incubated for an additional 48 h, and analyzed using a standard MTT assay. As shown in Figure 6 prodrug **4a** exhibited significantly enhanced dose-dependent antiproliferative activity against HeLa and A549 cells with high biotin receptor levels.[13] In conjunction with the results shown in Figure 5 and S8, these data also serve to confirm that the biotin moiety can guide prodrug **4a** to biotin receptor-positive HeLa and A549 tumor cells. Following S–S bond scission, this gives rise to the observed anti-proliferative activity as the result of releasing SN-38 within the cell. In contrast, the non-biotinylated prodrug **4b** did not show such specific antiproliferative activity; nor, was a dependence on biotin-receptor levels in different cell lines observed (Figure S9).

In an effort to assess whether drug release from **4a** would occur in tumor-affected tissues, a mouse xenograft model was used to evaluate tumor targeting and organ distribution. In these studies, HeLa tumor-bearing mice were treated with **4a** by intravenous injection (2.5 mg kg^{-1}). Ex vivo optical and fluorescence imaging was then carried out. A strong fluorescent signal was seen for the tumor-affected regions after treatment with **4a**. In contrast, only weak or negligible signals were seen in the case of other organs, including the liver, kidney, lung, and spleen (Figure 6a). Also tumor-selective enhancements in fluorescence were seen for cryo-sectioned tumor tissues obtained from mice injected with **4a** (Figure 6b). An appreciable fluorescence signal was seen only in the tissues bearing the HeLa tumor cells. Under similar conditions, the non-biotinylated prodrug **4b** did not give rise to a tumor specific biodistribution of wither the chemotherapeutic or imaging agents (Figure 6a, right side).

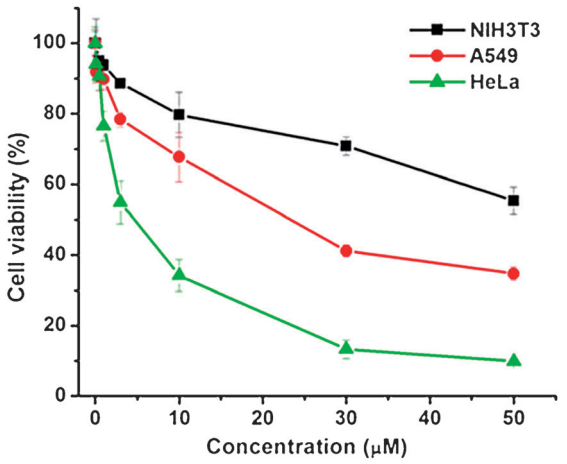

Figure 5. Cell viability of HeLa, A549, and NIH3T3 cells pretreated with various concentrations of prodrug **4a** in PBS. After treatment, the cells were incubated for 48 h. Cell viability was assessed using a standard MTT assay.

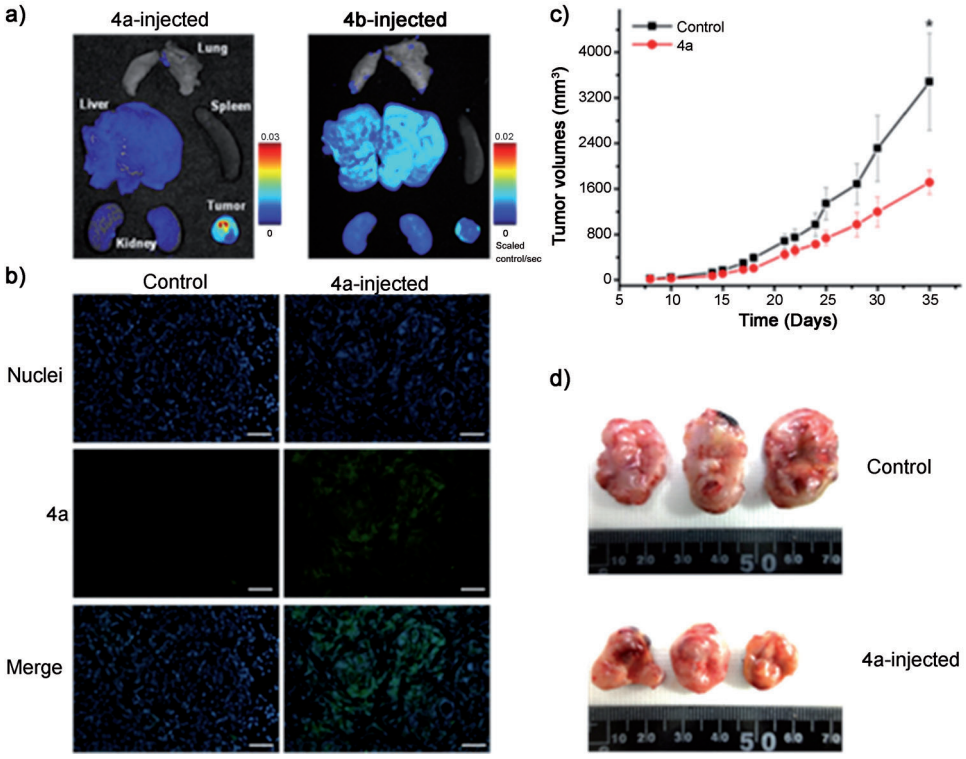

Figure 6. Ex vivo biodistribution of prodrugs (**4a**, **4b**) and in vivo therapeutic efficacy of prodrug **4a**. a) Fluorescent images of tumor region and major organs obtained from tumor-bearing nude mice after systemic injection of the animals with prodrug **4a** and **4b** in PBS. b) Fluorescent images of tumor tissues excised from mice treated with saline and prodrug **4a** (green, prodrug **4a**; blue, nuclei). Scale bar: 50 μm. Images were obtained using excitation wavelengths of 360 nm and 510 nm, and recording the output over the 440–500 nm and 540–600 nm spectral regions, for the blue and green signals, respectively. c) Time course of solid tumor volumes for HeLa cell mice xenografts. Prodrug **4a** was injected into the tail vein in 5 doses of 125 μg kg^{-1} each every other day starting day 10 after inoculation to induce the xenograft. d) Photographic images of the solid tumors excised from each group 35 days post initial inoculation of tumor cells.

Based on the above studies the tumor specific in vitro cellular uptake, imaging, antiproliferative activity, and biodistribution of **4a** (but not control **4b**) was considered confirmed. Therefore, the antitumor efficacy of **4a** was evaluated in vivo. This was done using a xenograft murine model created by subcutaneous inoculation with HeLa cells and measuring the extent of tumor growth (Figure 6c and d). In these studies, prodrug **4a** was administered every other day for a total of 5 doses of 125 $\mu g\,kg^{-1}$ each via tail vein injection starting at day 10 post-inoculation. Saline was used as a control. In the mice treated with **4a**, the tumor volume was significantly reduced compared with control group ($p < 0.05$ at day 35 post-inoculation). We take this as an indication that the biotinylated prodrug **4a** works according to design expectations in vivo as well as in vitro. Specifically, based on our findings we suggest that this cleavable theranostic 1) displays tumor-targeting features both in vitro and in vivo, 2) is able to deliver SN-38 into tumor cells, 3) allows visualization of cancerous lesions, and 4) exhibits antiproliferative activity in xenograft tumor models.

In conclusion, we report here a new theranostic agent, prodrug **4a**, which contains a biotinylated rhodol subunit (**1a**) as a fluorescent signaling moiety connected to a potent anticancer drug, SN-38, through a cleavable linker. The biotin functionality was expected to promote tumor targeting, while the specific choice of spacers was expected to allow for the enhanced release of both the active drug, SN-38, and the emissive rhodol moiety **1a** in thiol-containing intracellular milieus. The viability of the design was tested under controlled chemical conditions. For instance, as prepared, prodrug **4a** gives rise to a relatively weak fluorescence signal. However, exposure to GSH, but not a number of potential interferants, leads to a roughly 32-fold increase in the fluorescence intensity. Based on control studies involving precursor **3a**, an analogue of **4a** lacking the cytotoxic SN-38 payload, prodrug **4a** is internalized effectively within biotin receptor-enriched cells by receptor-mediated endocytosis. Considerably less uptake is seen in cells that are not enriched in the biotin receptor. In cells treated with **4a** an enhancement in fluorescence intensity ascribable to fluorophore **1a** is seen, with this increase correlating with the extent of cellular uptake. Evidence for the production of SN-38 in its free, active form was obtained from independent fluorometric analyses. On this basis it is concluded that the fluorescence of compound **1a**, which provides a signal that is much easier to monitor than that of SN-38, may be used to track conveniently the intracellular uptake and thiol-induced release of SN-38 from prodrug **4a**. Treatment with **4a** gave rise to anticancer effects in biotin receptor-positive cells. Moreover, fluorescent imaging analyses, carried out after intravenous injection of prodrug **4a** into mice containing HeLa cell xenografts served to confirm an increase in fluorescence. A statistically significant anticancer effect was also seen in these tumor models. On this basis, we conclude that prodrug **4a** and analogues represent a potentially useful new approach to theranostic design and represent species that could provide new tools for tumor-targeted drug delivery and concomitant monitoring of uptake and function by fluorescent imaging. To our knowledge, this is the first time these design principles have been successfully demonstrated both in vitro and in vivo.

Received: December 22, 2013
Revised: February 17, 2014
Published online: March 18, 2014

Keywords: biotin · cellular imaging · glutathione · SN-38 · theranostic

[1] E. S. Andersen, M. Dong, M. M. Nielsen, K. Jahn, R. Subramani, W. Mamdouh, M. M. Golas, B. Sander, H. Stark, C. L. P. Oliveira, J. S. Pedersen, V. Birkedal, F. Besenbacher, K. V. Gothelf, J. Kjems, *Nature* **2009**, *459*, 73.
[2] J. Decock, N. Obermajer, S. Vozelj, W. Hendrickx, R. Paridaens, J. Kos, *Int. J. Biol. Markers* **2008**, *23*, 161.
[3] N. Yamazaki, S. Kojima, N. V. Bovin, S. Andre, S. Gabius, H. J. Gabius, *Adv. Drug Delivery Rev.* **2000**, *43*, 225.
[4] a) S. H. Lee, J. Y. Kim, J. Ko, J. Y. Lee, J. S. Kim, *J. Org. Chem.* **2004**, *69*, 2902; b) Y. H. Lee, M. H. Lee, J. F. Zhang, J. S. Kim, *J. Org. Chem.* **2010**, *75*, 7159; c) H. J. Kim, J. S. Kim, *Tetrahedron Lett.* **2006**, *47*, 7051; d) J. S. Kim, H. J. Kim, H. M. Kim, S. H. Kim, J. W. Lee, S. K. Kim, B. R. Cho, *J. Org. Chem.* **2006**, *71*, 8016; e) K. C. Ko, J.-S. Wu, H. J. Kim, P. S. Kwon, J. W. Kim, R. A. Bartsch, J. Y. Lee, J. S. Kim, *Chem. Commun.* **2011**, *47*, 3165.
[5] S. Maiti, N. Park, J. H. Han, H. M. Jeon, J. H. Lee, S. Bhuniya, C. Kang, J. S. Kim, *J. Am. Chem. Soc.* **2013**, *135*, 4567.
[6] R. H. J. Mathijssen, R. J. vanAlphen, J. Verweij, W. J. Loos, K. Nooter, G. Stoter, A. Sparreboom, *Clin. Cancer Res.* **2001**, *7*, 2182.
[7] B. Gatto, G. Capranico, M. Palumbo, *Curr. Pharm. Des.* **1999**, *5*, 195.
[8] S. Chen, X. Zhao, J. Chen, J. Chen, L. Kuznetsova, S. S. Wong, I. Ojima, *Bioconjugate Chem.* **2010**, *21*, 979.
[9] B. C. Dickinson, C. J. Chang, *J. Am. Chem. Soc.* **2008**, *130*, 9638.
[10] J. A. Cook, H. I. Pass, S. N. Iype, N. Friedman, W. DeGraff, A. Russo, J. B. Mitchell, *Cancer Res.* **1991**, *51*, 4287.
[11] M. Qi, P. Wang, D. Wu, *Drug Dev. Ind. Pharm.* **2003**, *29*, 661.
[12] K. D. Brown, D. M. Blakeley, P. Roberts, R. J. Avery, *Biochem. J.* **1985**, *229*, 119.
[13] D. N. Heo, D. H. Yang, H. J. Moon, J. B. Lee, M. S. Bae, S. C. Lee, W. J. Lee, I. C. Sun, I. K. Kwon, *Biomaterials* **2012**, *33*, 856.
[14] N. Jiang, N. S. Tan, B. Ho, J. L. Ding, *Nat. Immunol.* **2007**, *8*, 1114.
[15] J. D. Gregory, *J. Am. Chem. Soc.* **1955**, *77*, 3922.
[16] J. Tomasina, S. Lheureux, P. Gauduchon, S. Rault, A. Malzert-Fréon, *Biomaterials* **2013**, *34*, 1073.

